Extended finite element method for dynamic fracture of piezo-electric materials

H. Nguyen-Vinh [a,b,c], I. Bakar [a,b,c], M.A. Msekh [a,b,c], J.-H. Song [a,b,c], J. Muthu [a,b,c], G. Zi [a,b,c], P. Le [a,b,c], S.P.A. Bordas [a,b,c,d], R. Simpson [a,b,c], S. Natarajan [a,b,c], T. Lahmer [a,b,c], T. Rabczuk [a,b,c,*]

[a] Department of Civil Engineering, Bauhaus University Weimar, Marienstr. 15, 99423 Weimar, Germany
[b] School of Mechanical, Industrial and Aeronautical Engineering, University of Witwatersrand, Johannesbuerg, South Africa
[c] Faculty of Civil Engineering, Universiti Teknologi Mara, 40450 Shah Alam, Selangor, Malaysia
[d] Institute of Mechanics & Advanced Materials (IMAM), School of Engineering, Cardiff University, Queen's Buildings The Parade, CARDIFF CF243AA, Waless, UK

ARTICLE INFO

ABSTRACT

We present an extended finite element formulation for dynamic fracture of piezo-electric materials. The method is developed in the context of linear elastic fracture mechanics. It is applied to mode I and mixed mode-fracture for quasi-steady cracks. An implicit time integration scheme is exploited. The results are compared to results obtained with the boundary element method and show excellent agreement.

1. Introduction

Piezo-electric materials are used as sensors, actuators or transducers in many engineering applications [7,8,18]. For an example, piezo-electric materials are used as an accelerator, distance or knock-sensors in automotive industry and as sonar transducers for navigation purposes. Piezo-electric transducers are applied extensively in medical engineering for destroying kidney stones and for plaque removal. However the limited knowledge about the fracture of these smart materials is essential for their effective use, particularly for applications with high stress concentrations applications, ex: ultrasound cleaning or valve control in common-rail diesel engines [26].

Studies on fracture of piezo-electric materials are limited to static applications using linear elastic fracture mechanics (LEFMs) [29,38,41]. The influence of permeable and impermeable boundary conditions was studied by Fan and Gao [15] and Shindo et al. [37]. Fracture criteria that take the influence of the electric field into account were done by Fulton and Gao [14], Gao et al. [16] and Park and Sun [30]. The fracture criterion of Park and Sun [30] agreed well with experimental results. Fulton and Gao [14] and Gao et al. [16] extended this criterion to non-linear effects and in [3] to fatigue cracks.

The extended finite element (XFEM) method was originally developed to model arbitrary crack growth without remeshing [5,25]. XFEM is based on a local partition of unity (PU) enrichment. The basic idea of XFEM is the enrichment of the finite element (FE)-interpolation with information of the analytical solution. For example, cracks will create discontinuities in the displacement field and therefore a discontinuous function such as the Heaviside-function or the step function is used as an enrichment function. It is also known that in LEFM, there exists a stress singularity at the crack tip. Sometimes, the near-crack tip solution is known and this information can be also included through the enrichment function in the

---

approximation. In the general case, these functions are not known a priori, and XFEM can be use equally well with numerically determined enrichment functions, as, for example in [44,45,46,47,48,49]. XFEM can be considered as an extension of the Partition of Unity Finite Element Method (PUFEM) [24] to discontinuous problems. Meanwhile, XFEM has been extended and applied to a variety of problems such as two-phase-flow [10,11], fluid–structure interaction [1,21,22,50,51] and thermo-mechanical problems [2] as well as moving boundary problems such as biofilm growth [52].

An XFEM-formulation for modeling the fracture of piezo-electric materials under static conditions using LEFM was presented by Béchet et al. [4]. They derived novel enrichment functions around the crack tip for the displacement and for the electric potential field. They also presented an efficient way to compute the generalized stress intensity factors. Verhoosel et al. [42] proposed a multiscale approach for modeling the fracture of piezo-electric materials based on cohesive cracks. An excellent overview article on modeling fracture of piezo-electric materials is given by Kuna [20]. Alternative methods to model intact piezo-electric materials including the Smoothed Finite Element Method (SFEM) [6,27,28] and meshfree methods [31] were presented by various authors. Note the recent work on enriched residual free bubble for coupled advection diffusion problems arising in nanoelectronics simulations [53]. Open source extended finite element codes in C++ [54] and enriched meshless method codes in MATLAB [55] are available for download.[1]

To our best knowledge, there are no studies concerning the dynamic behavior of piezoelectric materials using XFEM which are essential for utilizing smart materials for different engineering applications. In this paper, we present an extension of the work of Béchet et al. [4] to dynamic fracture of piezoelectric materials. We have developed the method using linear elastic fracture mechanics and it is validated by comparing numerical results with boundary element method (BEM) results.

1.1. Governing equations and weak form

The governing equations for the coupled electro-mechanical problem are given in weak form: Find $\mathbf{u} \in \mathcal{U} \ \forall \ \delta\mathbf{u} \in \mathcal{U}_0$ und $\mathbf{\Phi} \in \mathcal{V} \ \forall \ \delta\mathbf{\Phi} \in \mathcal{V}_0$ such that

$$\int_\Omega \sigma_{ij} \delta\epsilon_{ij} d\Omega - \int_\Omega b_i \delta u_i d\Omega - \int_{\Gamma_t} \bar{t}_i \delta u_i d\Gamma - \int_\Omega \varrho \ddot{u}_i \delta u_i d\Gamma = 0 \quad \forall \ \mathbf{x} \in \Omega \tag{1}$$

$$\int_\Omega D_i \delta E_i d\Omega - \int_{\Gamma_q} \delta\Phi \bar{q} d\Gamma = 0 \quad \forall \ \mathbf{x} \in \Omega \tag{2}$$

where σ_{ij} is the Cauchy-stress tensor, u_i the displacement field, b_i the body forces, t_i the traction and Φ the electric potential; δ denotes the 'variation' and an overline superimposed quantities, e.g $\bar{t}_i$ is the von Neumann traction. The domain is denoted by Ω with boundary Γ, where the indices u,t,q (Φ), and c denote 'displacement', 'traction', 'electric' and 'crack' boundaries, respectively, see Fig. 1. The approximation of the test and trial functions is given by

$$\mathcal{U} = \{\mathbf{u}|\mathbf{u} \in \mathcal{H}^1, \quad \mathbf{u} = \bar{\mathbf{u}} \text{ on } \Gamma_u, \quad \mathbf{u} \text{ discontinuous on } \Gamma_c\}$$
$$\mathcal{U}_0 = \{\delta\mathbf{u}|\delta\mathbf{u} \in \mathcal{H}^1, \quad \delta\mathbf{u} = 0 \text{ on } \Gamma_u, \quad \delta\mathbf{u} \text{ discontinuous on } \Gamma_c\}$$
$$\mathcal{V} = \{\Phi|\Phi \in \mathcal{H}^1, \quad \Phi = \overline{\Phi} \text{ on } \Gamma_q, \quad \Phi \text{ discontinuous on } \Gamma_c\}$$
$$\mathcal{V} = \{\delta\Phi|\delta\Phi \in \mathcal{H}^1, \quad \delta\Phi = 0 \text{ on } \Gamma_q, \quad \delta\Phi \text{ discontinuous on } \Gamma_c\} \tag{3}$$

where $\mathcal{H}^1$ denotes the first Hilbert space. The compatibility conditions and the constitutive model are imposed in strong form by

$$\epsilon_{ij} = 1/2(u_{i,j} + u_{j,i})$$
$$E_i = -\Phi_{,i}$$
$$\sigma_{ij} = C^E_{ijkl}\epsilon_{kl} - e_{kij}E_k$$
$$D_i = e_{ikl}\epsilon_{kl} + \kappa^\epsilon_{ik}E_k \tag{4}$$

where ϵ_{ij} is the strain tensor derived from the displacement field u_i, E_i is the electric field depending on the electric potential Φ, C^E_{ijkl} is the first-order elasticity tensor, κ^ϵ_{ik} is the dielectric Tensor and e_{kij} is the piezo-electric tensor.

2. XFEM for piezo-electric materials

The approximation of the displacement field in the XFEM [5,25,39,40] is given by

$$\mathbf{u}^h(\mathbf{x}) = \sum_{I \in \mathcal{S}} N_I(\mathbf{x})\mathbf{u}_I + \sum_{N=1}^{n_c}\sum_{I \in \mathcal{S}_c} N_I(\mathbf{x})\psi_I^{(N)}\mathbf{a}_I^{(N)} + \sum_{M=1}^{m_t}\sum_{I \in \mathcal{S}_t} N_I(\mathbf{x})\sum_{K=1}^{N_K}\phi_{KI}^{(M)}\mathbf{b}_{KI}^{(M)} \tag{5}$$

and in matrix form:

$$\mathbf{u}^h(\mathbf{X}) = \overline{\mathbf{N}}\overline{\mathbf{D}} + \widetilde{\mathbf{N}}\widetilde{\mathbf{D}} + \widehat{\mathbf{N}}\widehat{\mathbf{D}} \tag{6}$$
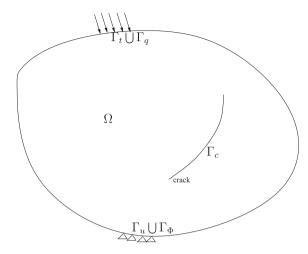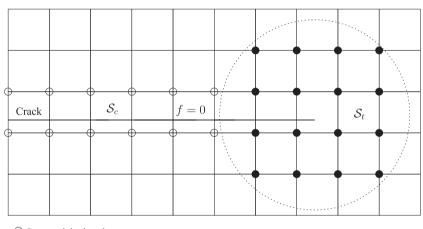
Fig. 1. Definitions.

○ Step enriched nodes

● Tip enriched nodes

Fig. 2. Enriched nodes and definitions.

where $\mathcal{S}$ is the set of all nodes, $\mathcal{S}_t$ is the set of nodes around the crack tip and $\mathcal{S}_c$ is the set of nodes for elements that are completely cut by the crack (Fig. 2); n_c denotes the number of cracks, $\psi_I^{(N)}$ is the associated enrichment function for discontinuity N, m_t is the number of crack tips and N_K is the number of enrichment functions in ϕ_{KI}; the unknowns $\mathbf{u}_I$, $\mathbf{a}_I$ and $\mathbf{b}_{KI}$ are stored in the vectors $\overline{\mathbf{D}}$, $\widetilde{\mathbf{D}}$ and $\widehat{\mathbf{D}}$.

We choose the step function as enrichment function in $\mathcal{S}_c$ that ensures the jump in the displacement field

$$\psi_{I,Riss}^{(N)} = sign[f^{(N)}(\mathbf{X})] - sign[f^{(N)}(\mathbf{X}_I)] \tag{7}$$

with

$$f^{(N)}(\mathbf{X}) = sign[\mathbf{n} \cdot (\mathbf{X} - \mathbf{X}^{(N)})]\underbrace{min(\mathbf{X} - \mathbf{X}^{(N)})}_{\mathbf{X}^N \in \Gamma_c^{(N)}} \tag{8}$$

where $\mathbf{n}$ is the normal of the crack. The second term on the RHS of Eq. (7) is called shifting and ensures that the enriched shape function $N_I(\mathbf{x})\psi_I^{(N)}$ vanishes in the blending element. The shifting also guarantees the Kronecker-delta property of the XFEM-interpolation. In other words: the nodal parameters $\mathbf{u}_I$ remain the physical displacements.

For electro-mechanical problems, Bechet et al. [4] have developed a crack tip enrichment function in 2D for LEFM problems. In this manuscript, we employ the standard mechanical enrichment function (Fig. 3)
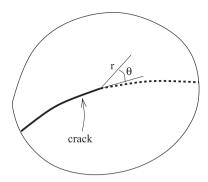
Fig. 3. Definitions for the crack tip enrichment.

$$\phi_{KI}^{mech} = \left[\sqrt{r}sin\frac{\theta}{2}, \sqrt{r}cos\frac{\theta}{2}, \sqrt{r}sin\frac{\theta}{2}sin\theta, \sqrt{r}cos\frac{\theta}{2}sin\theta \right] \tag{9}$$

and the electro-mechanical enrichment that has the form

$$\phi_{KI}^{piezo} = \left[\sqrt{r}f_1(\theta), \sqrt{r}f_2(\theta), \sqrt{r}f_3(\theta), \sqrt{r}f_4(\theta), \sqrt{r}f_5(\theta), \sqrt{r}f_6(\theta) \right] \tag{10}$$

as proposed by Béchet et al. [4]; more details on the complex enrichment functions f_i ($i = 1, \ldots, 6$) are given in [4]. The structure of the test-functions is similar:

$$\delta \mathbf{u}^h(\mathbf{X}) = \overline{\mathbf{N}}\delta\overline{\mathbf{D}} + \widetilde{\mathbf{N}}\delta\widetilde{\mathbf{D}} + \widehat{\mathbf{N}}\delta\widehat{\mathbf{D}} \tag{11}$$

The approximation of the electric potential is similar to the approximation of the displacement field:

$$\Phi^h(\mathbf{x}) = \sum_{I \in \mathcal{S}} N_I(\mathbf{x})\Phi_I + \sum_{N=1}^{n_c}\sum_{I \in \mathcal{S}_c} N_I(\mathbf{x})\psi_I^{(N)}\alpha_I^{(N)} + \sum_{M=1}^{m_t}\sum_{I \in \mathcal{S}_t} N_I(\mathbf{x})\sum_{K=1}^{N_K}\phi_{KI}^{(M)}\beta_{KI}^{(M)} \tag{12}$$

or in matrix form

$$\Phi^h(\mathbf{X}) = \overline{\mathbf{N}\Phi} + \widetilde{\mathbf{N}}\widetilde{\Phi} + \widehat{\mathbf{N}}\widehat{\Phi} \tag{13}$$

where the unknown $\Phi_I, \alpha_I^{(N)}$ and $\beta_{KI}^{(M)}$ are stored in the vectors $\overline{\Phi}, \widetilde{\Phi}$ and $\widehat{\Phi}$. The approximation of the test function reads:

$$\delta\Phi^h(\mathbf{X}) = \overline{\mathbf{N}}\delta\overline{\Phi} + \widetilde{\mathbf{N}}\delta\widetilde{\Phi} + \widehat{\mathbf{N}}\delta\widehat{\Phi} \tag{14}$$

The spatial derivatives of the trial functions are obtained by formal differentiation

$$\nabla \mathbf{u}^h(\mathbf{x}) = \sum_{I \in \mathcal{S}} \underbrace{\nabla N_I(\mathbf{x})}_{\overline{\mathbf{B}}}\mathbf{u}_I + \sum_{N=1}^{n_c}\sum_{I \in \mathcal{S}_c} \underbrace{\left(\nabla N_I(\mathbf{x})\psi_I^{(N)} + N_I(\mathbf{x})\nabla\psi_I^{(N)}\right)}_{\widetilde{\mathbf{B}}}\mathbf{a}_I^{(N)} + \sum_{M=1}^{m_t}\sum_{I \in \mathcal{S}_t} \underbrace{\left(\nabla N_I(\mathbf{x})\sum_{K=1}^{N_K}\phi_{KI}^{(M)} + N_I(\mathbf{x})\sum_{K=1}^{N_K}\nabla\phi_{KI}^{(M)}\right)}_{\widehat{\mathbf{B}}}\mathbf{b}_{KI}^{(M)}$$

$$\mathbf{E} = \nabla\Phi^h(\mathbf{x}) = \sum_{I \in \mathcal{S}} \underbrace{\nabla N_I(\mathbf{x})}_{\overline{\mathbf{B}}}\Phi_I + \sum_{N=1}^{n_c}\sum_{I \in \mathcal{S}_c} \underbrace{\left(\nabla N_I(\mathbf{x})\psi_I^{(N)} + N_I(\mathbf{x})\nabla\psi_I^{(N)}\right)}_{\widetilde{\mathbf{B}}}\alpha_I^{(N)} + \sum_{M=1}^{m_t}\sum_{I \in \mathcal{S}_t} \underbrace{\left(\nabla N_I(\mathbf{x})\sum_{K=1}^{N_K}\phi_{KI}^{(M)} + N_I(\mathbf{x})\sum_{K=1}^{N_K}\nabla\phi_{KI}^{(M)}\right)}_{\widehat{\mathbf{B}}}\beta_{KI}^{(M)} \tag{15}$$

that can be given in matrix form by

$$\nabla\mathbf{u}^h(\mathbf{X}) = \overline{\mathbf{B}}\,\overline{\mathbf{D}} + \widetilde{\mathbf{B}}\,\widetilde{\mathbf{D}} + \widehat{\mathbf{B}}\,\widehat{\mathbf{D}}$$
$$\mathbf{E} = \overline{\mathbf{B}\Phi} + \widetilde{\mathbf{B}}\,\widetilde{\Phi} + \widehat{\mathbf{B}}\,\widehat{\Phi} \tag{16}$$

Similarly, we obtain the derivatives of the test functions:

$$\nabla\delta\mathbf{u}^h(\mathbf{X}) = \overline{\mathbf{B}}\delta\overline{\mathbf{D}} + \widetilde{\mathbf{B}}\delta\widetilde{\mathbf{D}} + \widehat{\mathbf{B}}\delta\widehat{\mathbf{D}}$$
$$\delta\mathbf{E} = \overline{\mathbf{B}}\delta\overline{\Phi} + \widetilde{\mathbf{B}}\delta\widetilde{\Phi} + \widehat{\mathbf{B}}\delta\widehat{\Phi} \tag{17}$$

3. Discrete equations

The discrete equations are obtained by substituting the approximations of the test and trial-functions, Eqs. (6), (11), (13) and (14), and their derivatives, Eqs. (16) and (17), into the weak form, Eqs. (1) and (2). With the compatibility condition and the constitutive model, Eq. (4), we obtain

$$\sum_{e=1}^{numele} \int_{\Omega^{(e)}} ([\overline{\mathbf{B}}\delta\overline{\mathbf{D}} + \widetilde{\mathbf{B}}\delta\widetilde{\mathbf{D}} + \widehat{\mathbf{B}}\delta\widehat{\mathbf{D}}]^{sym})^T [\mathbf{C}^E(\overline{\mathbf{B}}\,\overline{\mathbf{D}} + \widetilde{\mathbf{B}}\widetilde{\mathbf{D}} + \widehat{\mathbf{B}}\widehat{\mathbf{D}})^{sym} - \mathbf{e}(\overline{\mathbf{B}}\overline{\boldsymbol{\Phi}} + \widetilde{\mathbf{B}}\widetilde{\boldsymbol{\Phi}} + \widehat{\mathbf{B}}\widehat{\boldsymbol{\Phi}})]d\Omega$$

$$- \sum_{e=1}^{numele} \int_{\Omega^{(e)}} [\overline{\mathbf{N}}\delta\overline{\mathbf{D}} + \widetilde{\mathbf{N}}\delta\widetilde{\mathbf{D}} + \widehat{\mathbf{N}}\delta\widehat{\mathbf{D}}]^{\mathbf{T}}\mathbf{bd}\Omega - \sum_{\mathbf{e=1}}^{\mathbf{numrand_t}} \int_{\Gamma_{\mathbf{t}}^{(\mathbf{e})}} [\overline{\mathbf{N}}\delta\overline{\mathbf{D}} + \widetilde{\mathbf{N}}\delta\widetilde{\mathbf{D}} + \widehat{\mathbf{N}}\delta\widehat{\mathbf{D}}]^{\mathbf{T}}\mathbf{td}\Gamma$$

$$- \sum_{\mathbf{e=1}}^{\mathbf{numele}} \int_{\Omega^{(\mathbf{e})}} \varrho[\overline{\mathbf{N}}\delta\overline{\mathbf{D}} + \widetilde{\mathbf{N}}\delta\widetilde{\mathbf{D}} + \widehat{\mathbf{N}}\delta\widehat{\mathbf{D}}]^{\mathbf{T}}[\overline{\mathbf{N}}\ddot{\overline{\mathbf{D}}} + \widetilde{\mathbf{N}}\ddot{\widetilde{\mathbf{D}}} + \widehat{\mathbf{N}}\ddot{\widehat{\mathbf{D}}}]\mathbf{d}\Omega = \mathbf{0}$$

$$\sum_{\mathbf{e=1}}^{\mathbf{numele}} [\overline{\mathbf{B}}\delta\overline{\boldsymbol{\Phi}} + \widetilde{\mathbf{B}}\delta\widetilde{\boldsymbol{\Phi}} + \widehat{\mathbf{B}}\delta\widehat{\boldsymbol{\Phi}}]^{\mathbf{T}}[\mathbf{e}(\overline{\mathbf{B}}\,\overline{\mathbf{D}} + \widetilde{\mathbf{B}}\widetilde{\mathbf{D}} + \widehat{\mathbf{B}}\widehat{\mathbf{D}})^{\mathbf{sym}} + \boldsymbol{\kappa}(\overline{\mathbf{B}}\overline{\boldsymbol{\Phi}} + \widetilde{\mathbf{B}}\widetilde{\boldsymbol{\Phi}} + \widehat{\mathbf{B}}\widehat{\boldsymbol{\Phi}})]\mathbf{d}\Omega$$

$$- \sum_{\mathbf{e=1}}^{\mathbf{numrand_q}} \int_{\Gamma_{\mathbf{q}}^{(\mathbf{e})}} [\overline{\mathbf{N}}\delta\overline{\boldsymbol{\Phi}} + \widetilde{\mathbf{N}}\delta\widetilde{\boldsymbol{\Phi}} + \widehat{\mathbf{N}}\delta\widehat{\boldsymbol{\Phi}}]^{\mathbf{T}}\mathbf{q\,d}\Gamma = \mathbf{0} \tag{18}$$

where *numele* is the number of elements in the domain Ω and *numrand$_t$* and *numrand$_q$* are the number of boundary elements in Γ_t, Γ_q, respectively; *sym* denotes the symmetric part of a tensor. Defining

$$\mathbf{D} = [\overline{\mathbf{D}}, \widetilde{\mathbf{D}}, \widehat{\mathbf{D}}, \overline{\boldsymbol{\Phi}}, \widetilde{\boldsymbol{\Phi}}, \widehat{\boldsymbol{\Phi}}]^T$$
$$\delta\mathbf{D} = [\delta\overline{\mathbf{D}}, \delta\widetilde{\mathbf{D}}, \delta\widehat{\mathbf{D}}, \delta\overline{\boldsymbol{\Phi}}, \delta\widetilde{\boldsymbol{\Phi}}, \delta\widehat{\boldsymbol{\Phi}}]^T \tag{19}$$

and factoring out the nodal parameters of the test functions gives after some algebra the final (semi-) discrete system of equations:

$$\delta\mathbf{D}(\mathbf{M}\ddot{\mathbf{D}} + \mathbf{C}\dot{\mathbf{D}} + \mathbf{K}\mathbf{D} - \mathbf{F}) = 0 \tag{20}$$

with

$$\mathbf{M} = \begin{bmatrix} \mathbf{M}_{mm} & \mathbf{0} \\ \mathbf{0} & \mathbf{0} \end{bmatrix}; \quad \mathbf{C} = \begin{bmatrix} \mathbf{C}_{mm} & \mathbf{C}_{me} \\ \mathbf{C}_{em} & \mathbf{C}_{ee} \end{bmatrix}; \quad \mathbf{K} = \begin{bmatrix} \mathbf{K}_{mm} & \mathbf{K}_{me} \\ \mathbf{K}_{em} & \mathbf{K}_{ee} \end{bmatrix} \tag{21}$$

and the following sub-matrices for the mass

$$\mathbf{M}_{mm} = \begin{bmatrix} \mathbf{M}_{mm}^{uu} & \mathbf{M}_{mm}^{ua} & \mathbf{M}_{mm}^{ub} \\ \mathbf{M}_{mm}^{au} & \mathbf{M}_{mm}^{aa} & \mathbf{M}_{mm}^{ab} \\ \mathbf{M}_{mm}^{bu} & \mathbf{M}_{mm}^{ba} & \mathbf{M}_{mm}^{bb} \end{bmatrix} \tag{22}$$

the stiffness

$$\mathbf{K}_{ij} = \begin{bmatrix} \mathbf{K}_{ij}^{uu} & \mathbf{K}_{ij}^{ua} & \mathbf{K}_{ij}^{ub} \\ \mathbf{K}_{ij}^{au} & \mathbf{K}_{ij}^{aa} & \mathbf{K}_{ij}^{ab} \\ \mathbf{K}_{ij}^{bu} & \mathbf{K}_{ij}^{ba} & \mathbf{K}_{ij}^{bb} \end{bmatrix}, \quad i,j = m,e \tag{23}$$

and

$$\mathbf{M}_{mm}^{uu} = \int_{\Omega} \varrho\mathbf{N}_I\mathbf{N}_J d\Omega$$

$$\mathbf{M}_{mm}^{ua} = \int_{\Omega} \varrho\mathbf{N}_I\psi_J^{(N)}\mathbf{N}_J d\Omega = \mathbf{M}^{au}$$

$$\mathbf{M}_{mm}^{ub} = \int_{\Omega} \varrho\mathbf{N}_I\Phi_K^{(M)}\mathbf{N}_J d\Omega = \mathbf{M}_{mm}^{bu}$$

$$\mathbf{M}_{mm}^{aa} = \int_{\Omega} \varrho\mathbf{N}_I\psi_I^{(N)}\mathbf{N}_J\psi_J^{(N)} d\Omega$$

$$\mathbf{M}_{mm}^{ab} = \int_{\Omega} \varrho\mathbf{N}_I\Phi_K^{(M)}\mathbf{N}_J\psi_J^{(N)} d\Omega = \mathbf{M}_{mm}^{ba}$$

$$\mathbf{M}_{mm}^{bb} = \int_{\Omega} \varrho\mathbf{N}_I\Phi_K^{(M)}\mathbf{N}_J\Phi_K^{(M)} d\Omega \tag{24}$$

$$\mathbf{K}_{mm}^{uu} = \int_{\Omega} \mathbf{B}_I \mathbf{C} \mathbf{B}_J d\Omega$$

$$\mathbf{K}_{mm}^{ua} = \int_{\Omega} \mathbf{B}_I \mathbf{C} \mathbf{B}_J \psi_J^{(N)} d\Omega = \mathbf{K}_{mm}^{au}$$

$$\mathbf{K}_{mm}^{ub} = \int_{\Omega} \mathbf{B}_I \mathbf{C} \mathbf{B}_J \Phi_K^{(M)} d\Omega = \mathbf{K}_{mm}^{bu}$$

$$\mathbf{K}_{mm}^{aa} = \int_{\Omega} \psi_I^{(N)} \mathbf{B}_I \mathbf{C} \mathbf{B}_J \psi_J^{(N)} d\Omega$$

$$\mathbf{K}_{mm}^{ab} = \int_{\Omega} \psi_I^{(N)} \mathbf{B}_I \mathbf{C} \mathbf{B}_J \Phi_K^{(M)} d\Omega = \mathbf{K}_{mm}^{ba}$$

$$\mathbf{K}_{mm}^{bb} = \int_{\Omega} \Phi_K^{(M)} \mathbf{B}_I \mathbf{C} \mathbf{B}_J \Phi_K^{(M)} d\Omega \tag{25}$$

$$\mathbf{K}_{me}^{uu} = \int_{\Omega} \mathbf{B}_I \mathbf{e} \mathbf{B}_J d\Omega$$

$$\mathbf{K}_{me}^{ua} = \int_{\Omega} \mathbf{B}_I \mathbf{e} \mathbf{B}_J \psi_J^{(N)} d\Omega = \mathbf{K}_{mm}^{au}$$

$$\mathbf{K}_{me}^{ub} = \int_{\Omega} \mathbf{B}_I \mathbf{e} \mathbf{B}_J \Phi_K^{(M)} d\Omega = \mathbf{K}_{mm}^{bu}$$

$$\mathbf{K}_{me}^{aa} = \int_{\Omega} \psi_I^{(N)} \mathbf{B}_I \mathbf{e} \mathbf{B}_J \psi_J^{(N)} d\Omega$$

$$\mathbf{K}_{me}^{ab} = \int_{\Omega} \psi_I^{(N)} \mathbf{B}_I \mathbf{e} \mathbf{B}_J \Phi_K^{(M)} d\Omega = \mathbf{K}_{mm}^{ba}$$

$$\mathbf{K}_{me}^{bb} = \int_{\Omega} \Phi_K^{(M)} \mathbf{B}_I \mathbf{e} \mathbf{B}_J \Phi_K^{(M)} d\Omega \tag{26}$$

$$\mathbf{K}_{em}^{uu} = \int_{\Omega} \mathbf{B}_I \mathbf{e} \mathbf{B}_J d\Omega$$

$$\mathbf{K}_{em}^{ua} = \int_{\Omega} \mathbf{B}_I \mathbf{e} \mathbf{B}_J \psi_J^{(N)} d\Omega = \mathbf{K}_{mm}^{au}$$

$$\mathbf{K}_{em}^{ub} = \int_{\Omega} \mathbf{B}_I \mathbf{e} \mathbf{B}_J \Phi_K^{(M)} d\Omega = \mathbf{K}_{mm}^{bu}$$

$$\mathbf{K}_{em}^{aa} = \int_{\Omega} \psi_I^{(N)} \mathbf{B}_I \mathbf{e} \mathbf{B}_J \psi_J^{(N)} d\Omega$$

$$\mathbf{K}_{em}^{ab} = \int_{\Omega} \psi_I^{(N)} \mathbf{B}_I \mathbf{e} \mathbf{B}_J \Phi_K^{(M)} d\Omega = \mathbf{K}_{mm}^{ba}$$

$$\mathbf{K}_{em}^{bb} = \int_{\Omega} \Phi_K^{(M)} \mathbf{B}_I \mathbf{e} \mathbf{B}_J \Phi_K^{(M)} d\Omega \tag{27}$$

$$\mathbf{K}_{ee}^{uu} = \int_{\Omega} \mathbf{B}_I \boldsymbol{\kappa} \mathbf{B}_J d\Omega$$

$$\mathbf{K}_{ee}^{ua} = \int_{\Omega} \mathbf{B}_I \boldsymbol{\kappa} \mathbf{B}_J \psi_J^{(N)} d\Omega = \mathbf{K}_{mm}^{au}$$

$$\mathbf{K}_{ee}^{ub} = \int_{\Omega} \mathbf{B}_I \boldsymbol{\kappa} \mathbf{B}_J \Phi_K^{(M)} d\Omega = \mathbf{K}_{mm}^{bu}$$

$$\mathbf{K}_{ee}^{aa} = \int_{\Omega} \psi_I^{(N)} \mathbf{B}_I \boldsymbol{\kappa} \mathbf{B}_J \psi_J^{(N)} d\Omega$$

$$\mathbf{K}_{ee}^{ab} = \int_{\Omega} \psi_I^{(N)} \mathbf{B}_I \boldsymbol{\kappa} \mathbf{B}_J \Phi_K^{(M)} d\Omega = \mathbf{K}_{mm}^{ba}$$

$$\mathbf{K}_{ee}^{bb} = \int_{\Omega} \Phi_K^{(M)} \mathbf{B}_I \boldsymbol{\kappa} \mathbf{B}_J \Phi_K^{(M)} d\Omega \tag{28}$$

where the superimposed indices e and m indicate *electrical* and *mechanical* quantities, superscript u, a and b refer to 'usual', 'step-enriched' and 'tip-enriched' nodes and capital indices refer to node numbers. For many applications, it is sufficient to neglect the coupled damping terms and the electrical damping $\mathbf{C}^{me}$, $\mathbf{C}^{em}$ and $\mathbf{C}^{ee}$, but instead use only the mechanical Rayleigh-damping [23]:

$$\mathbf{C}^{mm} = \gamma \mathbf{K}^{mm} + \theta \mathbf{M}^{mm} \tag{29}$$

The semi-discrete equations are integrated in time using the implicit β-Newmark scheme. More details regarding time integration in XFEM are given by Cavin et al. [9], Combescure et al. [12], Réthoré et al. [35,36].

4. Computation of the stress intensity factors

The stress intensity factors (SIFs) can be evaluated through the displacement field and the electrical field or the crack opening displacement, for a discussion see De Luycker et al. [13], Garcia-Sanchez et al. [17], Wünsche et al. [43]. Alternatively, they can be obtained through the J-integral or the interaction integral. For a piezo-electric material, the domain form of the dynamic J-integral can be written as

$$J = \int_{A_{(\Gamma)}} \left(\sigma_{ij} \frac{\partial u_i}{\partial x_1} + D_j \frac{\partial \Phi}{\partial x_1} - H \delta_{1j} \right) \frac{\partial q}{\partial x_j} dA + \int_{A_{(\Gamma)}} \left(\rho \ddot{u}_i \frac{\partial u_i}{\partial x_1} - \rho \dot{u}_i \frac{\partial u_i}{\partial x_1} \right) q \, dA \tag{30}$$

where H is the electric enthalpy density for electromechanical loading, q is a smooth function chosen to be unity at the crack tip and n_j is the j_{th} component of the outward unit vector normal to an arbitrary contour Γ enclosing the crack tip. For linear piezoelectric solids under mixed-mode loading conditions, the relation of the stress intensity factors (SIFs) and the J-integral can be written as [19]

$$J = \frac{1}{2} \mathbf{K}^T \mathbf{Y} \mathbf{K} \tag{31}$$

where $K = (K_{II} \ K_I \ K_{III} \ K_{IV})$ is the vector of the four field intensity factors, and $\mathbf{Y}$ is the Irwin matrix for piezo-electric materials:

$$\mathbf{Y} = \begin{bmatrix} Y_{11} & Y_{12} & Y_{13} & Y_{14} \\ Y_{21} & Y_{22} & Y_{23} & 0 \\ Y_{31} & Y_{32} & Y_{33} & 0 \\ Y_{41} & 0 & 0 & Y_{44} \end{bmatrix} \tag{32}$$

The Irwin matrix is basically derived from the constitute relationship with the boundary conditions $\bar{t}_i = 0$ and $n_i D_i = 0$ on Γ_c. The left upper 3×3 matrix refers to the mechanical behavior of the piezo-electric material, Y_{44} is related to the permittivity and $Y_{14} = Y_{41}$ to the piezo-electricity. More details can be found in the excellent paper by Suo et al. [41].

The stress intensity factors K_I, K_{II} and K_{III} refer to the crack opening mode, crack sliding mode and tearing mode, respectively. The SIF K_{IV}, also called the electric displacement intensity factor, characterizes the concentration of the electrical displacement fields. Note that in a two-dimensional setting, the SIF K_{III} vanishes.

The drawback of the J-integral is that it can only be converted into single mode stress intensity factors. However, the crack is generally subjected to a mixed mode loading conditions with an additional electrical mode IV. A possibility in overcoming the limitation is given by the interaction integral method which is based on two load cases: (1) defines the actual loading of the structure and is assumed to be an auxiliary fields on the entire domain and (2) represents the electromechanical loading along a vanishingly small contour around the crack tip. The interaction integral for a homogeneous piezoelectric material is defined as [34]

$$I^{(1,2)} = \int_{A_{(\Gamma)}} \left(\sigma_{ij}^{(1)} \frac{\partial u_i^{(2)}}{\partial x_1} + D_j^{(1)} \frac{\partial \Phi^{(2)}}{\partial x_1} + \sigma_{ij}^{(2)} \frac{\partial u_i^{(1)}}{\partial x_1} + D_j^{(2)} \frac{\partial \Phi^{(1)}}{\partial x_1} - H^{(1,2)} \delta_{1j} \right) \frac{\partial q}{\partial x_j} \, dA$$
$$+ \int_{A_{(\Gamma)}} \left(\varrho \ddot{u}_i^{(1)} \frac{\partial u_i^{(2)}}{\partial x_1} - \varrho \dot{u}_i^{(1)} \frac{\partial u_i^{(2)}}{\partial x_1} + \varrho \ddot{u}_i^{(2)} \frac{\partial u_i^{(1)}}{\partial x_1} - \varrho \dot{u}_i^{(2)} \frac{\partial u_i^{(1)}}{\partial x_1} \right) q \, dA \tag{33}$$

with

$$H^{(1,2)} = \frac{\sigma_{ij}^{(1)} \epsilon_{ij}^{(2)} + \sigma_{ij}^{(2)} \epsilon_{ij}^{(1)} - D_j^{(1)} E_j^{(2)} - D_j^{(2)} E_j^{(1)}}{2} \tag{34}$$

The stress intensity factor can be defined as

$$I^{(1,2)} = K_{II}^{(1)} K_{II}^{(2)} Y_{11} + K_I^{(1)} K_I^{(2)} Y_{22} + K_{IV}^{(1)} K_{IV}^{(2)} Y_{44} + \left(K_I^{(1)} K_{II}^{(2)} + K_{II}^{(1)} K_I^{(2)} \right) Y_{12} + \left(K_{II}^{(1)} K_{IV}^{(2)} + K_{IV}^{(1)} K_{II}^{(2)} \right) Y_{14}$$
$$+ \left(K_I^{(1)} K_{IV}^{(2)} + K_{IV}^{(1)} K_I^{(2)} \right) Y_{24} \tag{35}$$

The SIFs are then obtained by judiciously choosing the auxiliary state in a way that two SIFs vanish and one is set to 1. More details are found in the excellent paper by Rao and Kuna [34].
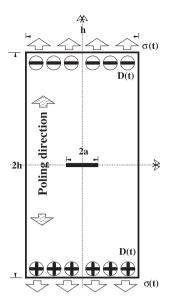
Fig. 4. Set up of the center crack problem.

5. Examples

5.1. Center crack

Let us consider a plate with a center crack under impact loading as illustrated in Fig. 4 with h = 40 mm and a = 2.4 mm. Plain strain conditions are assumed. The impact is caused either by a mechanical loading $\bar{\sigma}(t)$ or by an electrical loading $\overline{D}(t)$ or by a combination of both as shown in Fig. 4. This problem has been studied previously by Garcia-Sanchez et al. [17] in the context of the BEM and is used here as a validation example. They assumed a homogeneous linear piezo-electric solid with the following material parameters: C_{11} = 126 GPa; C_{12} = 84.1 GPa and C_{22} = 117 GPa and C_{66} = 23 GPa; e_{21} = 6.5 C/m^2, e_{22} = 23.3 C/m^2 and e_{16} = 17 C/m^2; κ_{11} = 15.04 C/(GV m) and e_{22} = 13 C/(GV m); density ϱ = 7500 kg/m^3. In order to facilitate a direct comparison, we adopt the presentation of the results in [17] who introduced normalized dynamic stress intensity factors and a normalized dynamic electrical displacement intensity factor:

$$K_I^* = \frac{K_I(t)}{K_I^{st}}, \quad K_{IV}^* = \Lambda \frac{K_{IV}(t)}{K_{IV}^{st}} \tag{36}$$

with

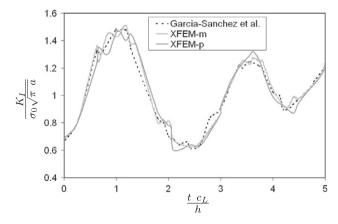$$\Lambda = \frac{e_{22}}{\kappa_{22}}, \quad K_I^{st} = \sigma_0\sqrt{\pi a} \tag{37}$$

Fig. 5. Normalized dynamic K_I factor for the mode I-fracture problem Section 5.1 compared to the results in [17], λ = 1; XFEM-m refers to a mechanical tip enriched XFEM formulation, Eq. (9); XFEM-p refers to a 'piezo-electric' tip enriched XFEM formulation as proposed by Bechet et al. [4].
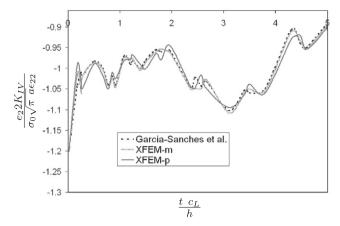
Fig. 6. Normalized dynamic K_{IV} factor for the mode I-fracture problem Section 5.1 compared to the results in [17], $\lambda = 1$; XFEM-m refers to a mechanical tip enriched XFEM formulation, Eq. (9); XFEM-p refers to a 'piezo-electric' tip enriched XFEM formulation as proposed by Bechet et al. [4].

Moreover, the ratio between electric impact and mechanical impact is defined as

$$\lambda = \Lambda \frac{D_{22}}{\sigma_{22}} \tag{38}$$

The plate is discretized with different refinements on Cartesian grids using standard 4-node elements starting from approximately 1500 elements up to almost 12,000 (155×76) elements. At least 77×38 elements were needed in order to obtain convergent results. Afterwards, the results were very similar. As an analytical solution is not available and therefore a thorough convergence study cannot be performed, we present only the results for 77×38 elements in this manuscript. We also ensured that the time step has no critical influence on the numerical results. Though it would reduce computational costs, no symmetry conditions have been used.

Figs. 5 and 6 compare the results obtained with XFEM to the results of the BEM obtained in [17]. Therefore, we have adopted the illustration from Garcia-Sanchez et al. [17] and presented the results in normalized form where c_L is the longitudinal wave speed. The results agree reasonably well. The results of XFEM with pure 'mechanical' tip enrichment (XFEM-m), Eq. (9), are also compared with the results of an XFEM-formulation using the enrichment proposed by Bechet et al. [4] (XFEM-p). There are only minor differences in the results. We note that the key advantage of XFEM is its ability to model crack growth without re-meshing. This capability can also be used in the context of inverse analysis where the detection of cracks or inclusions in piezo-electric materials is of interest. However, in this manuscript, our main goal is to develop a dynamics XFEM-formulation for stationary cracks.

Fig. 7 shows the influence of the electrical impact intensity on the results. For dynamic problems, the dynamic stress intensity factor is larger than the static stress intensity factor. It can also be seen that an electric impact can cause negative values of the dynamic stress intensity factor. The maximum values of the normalized dynamic stress intensity factor is reduced with increasing λ-value, i.e. increasing influence of electrical impact. Fig. 8 shows the results for a pure electrical impact when the direction of impact is reversed. The magnitudes of the normalized dynamic stress intensity factor remain the same but the signs change, meaning that change in the direction of the impact does not cause the absolute value of the dynamic stress intensity factor to change.
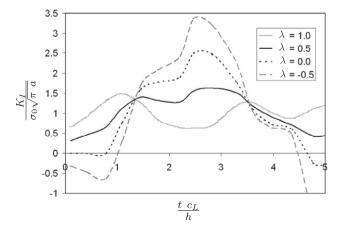

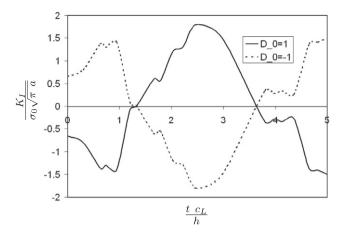**Fig. 7.** Normalized dynamic K_I factor for the mode I-fracture problem Section 5.1 for different λ-values.

Fig. 8. Effect of the direction of electrical impact on the normalized dynamic K_I-factor for the mode I-fracture problem Section 5.1.
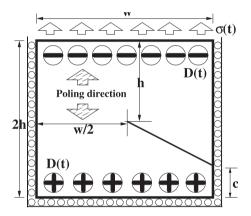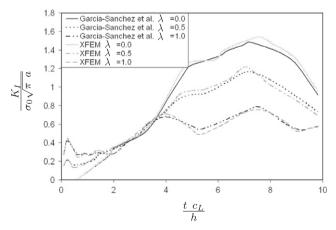

Fig. 9. Set up of the slanter crack problem.

Fig. 10. Normalized dynamic K_I factor for the slanted crack problem for different λ-values.

5.2. Slanted crack

The last example was also extracted from Garcia-Sanchez et al. [17]. Therefore, consider a homogeneous and linear piezo-electric specimen that contains a slanted crack as shown in Fig. 9 with $h = 22$ mm, $w = 32$ mm, $c = 6$ mm and $a = 22.63$ mm. Plain strain conditions are assumed and the material parameters from the previous section are used. We tested again differ-ent refinements as in the previous example and achieved convergence with 4000 elements, which agrees well with the
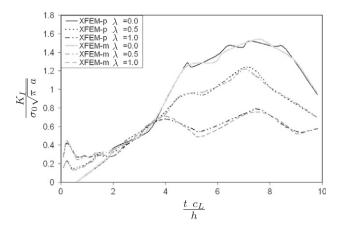
Fig. 11. Normalized dynamic K_I factor for the slanted crack problem for different λ-values. Comparison between XFEM with pure 'mechanical' tip enrichment, Eq. (9), XFEM-m versus XFEM with 'piezo-electric' tip enrichment [4], XFEM-p.

Fig. 12. Normalized dynamic K_{II} factor for the slanted crack problem for different λ-values.

Fig. 13. Normalized dynamic K_{II} factor for the slanted crack problem for different λ-values. Comparison between XFEM with pure 'mechanical' tip enrichment, Eq. (9), XFEM-m versus XFEM with 'piezo-electric' tip enrichment [4], XFEM-p.
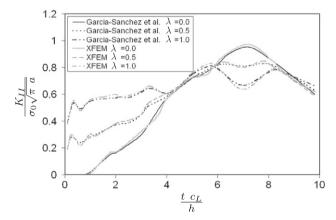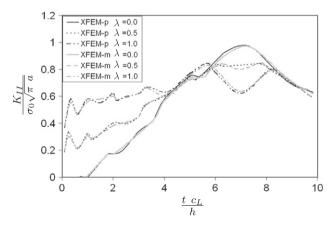
previous results. Therefore, we present only results of a discretization with $75 \times 54(=4050)$ elements and compare those to the BEM results presented in Garcia-Sanchez et al. [17].

Fig. 10 shows the normalized dynamic stress intensity factor K_I for different values of λ. The results agree well with those obtained in Garcia-Sanchez et al. [17]. The same observations are made when comparisons are done with the normalized dynamic stress intensity factor K_{II}, Fig. 12. Comparisons between different tip-enrichments (XFEM-m versus XFEM-p) are

illustrated in Figs. 11 and 13. The differences are minor. One can also observe that the electrical impact has in general a 'positive' effect on the normalized dynamic stress intensity factor. In other words, both, K_I^* as well as K_{II}^* decrease with increasing λ.

6. Conclusion

We have presented an extended finite element method for dynamic fracture of piezo-electric materials. The method exploits the partition of unity enrichment and therefore allows crack propagation without remeshing. It can be considered as an extension of the method by Bechet et al. [4] to dynamics. The β-Newmark implicit time integration scheme is adopted.

We have tested different crack tip enrichment functions, i.e. the pure mechanical enrichment function and the more complex enrichment function from Bechet et al. [4] for piezo-electric materials. We found that the results differ only slightly when the more complex enrichment functions from Bechet et al. [4] are used. However it is not possible to make a general statement regarding the accuracy as there are no analytical solutions for dynamic problems of piezo-electric materials.

The method was applied to two examples with mechanical and electrical boundary conditions, that concern with quasi-steady cracks. Since no analytical results are available for dynamic fracture problems of piezo-electric materials, the XFEM results were compared to results obtained by the BEM [17] and they show excellent agreement.

In the future, we will extend the method to non-linear materials involving cohesive cracks and inverse problems, i.e. to detect inclusions and cracks in piezo-electric materials. XFEM seems to be ideally suited for inverse problems as shown by [32,33].

Acknowledgement

References

[1] Zilian A, Legay A. The enriched space–time finite element method (est) for simultaneous solution of fluid–structure interaction. Int J Numer Methods Eng 2008;75:305–34.
[2] Areias PMA, Belytschko T. Two-scale method for shear bands: thermal effects and variable bandwidth. Int J Numer Methods Eng 2007;72:658–96.
[3] Arias I, Serebrinsky S, Ortiz M. A phenomenological cohesive model of ferroelectric fatigue. Acta Mater 2006;54:975–84.
[4] Bechet E, Scherzer M, Kuna M. Application of the X-FEM to the fracture of piezoelectric materials. Int J Numer Methods Eng 2009;77:1535–65.
[5] Belytschko T, Black T. Elastic crack growth in finite elements with minimal remeshing. Int J Numer Methods Eng 1999;45(5):601–20.
[6] Bordas S, Rabczuk T, Nguyen-Xuan H, Nguyen VP, Natarajan S, Bog T, et al. Strain smoothing in FEM and XFEM. Comput Struct 2010;88(23–24):1419–43.
[7] Cady WG. Piezoelectricity – an introduction to the theory and applications of electromechanical phenomena in crystals, vol. 1. Dover Publications, Inc.; 1964.
[8] Cady WG. Piezoelectricity – an introduction to the theory and applications of electromechanical phenomena in crystals, vol. 2. Dover Publications, Inc.; 1964.
[9] Cavin P, Gravouil A, Lubrecht AA, Combescure A. Automatic energy conserving space–time refinement for linear dynamic structural problems. Int J Numer Methods Eng 2005.
[10] Chessa J, Belytschko T. An enriched finite element method and level sets for axisymmetric two-phase flow with surface tension. Int J Numer Methods Eng 2003;58(13):2041–64.
[11] Chessa J, Belytschko T. An extended finite element method for two-phase fluids. ASME J Appl Mech 2003;70:1017.
[12] Combescure A, Gravouil A, Gregoire D, Réthoré J. X-FEM a good candidate for energy conservation in simulation of brittle dynamic crack propagation. Comput Methods Appl Mech Eng; 2007.
[13] De Luycker E, Benson DJ, Belytschko T, Bazilevs Y, Hsu MC. X-FEMIN isogeometric analysis for linear fracture mechanics. Int J Numer Methods Eng; in press.
[14] Fulton CC, Gao HJ. Electrical nonlinearity in fracture of piezoelectric ceramics. Appl Mech Rev 1997;50:5663.
[15] Fan WX, Gao CF. Exact solutions for the plane problem in piezoelectric materials with an elliptic or a crack. Int J Solids Struct 1999;36:2527–40.
[16] Gao H, Zhang TY, Tong P. Local and global energy release rates for an electrically yielded crack in a piezoelectric ceramic. J Mech Phys Solids 1997;45:491–510.
[17] Garcia-Sanchez F, Zhang C, Saez A. 2-d transient dynamic analysis of cracked piezoelectric solids by a time-domain BEM. Comput Methods Appl Mech Eng 2008;197:3108–21.
[18] Ikeda T. Fundamentals of piezoelectricity. Oxford University Press; 1990.
[19] Kuna M. Finite element analyses of cracks in piezoelectric structures: a survey. Arch Appl Mech 2006;76:725–45.
[20] Kuna M. Fracture mechanics of piezoelectric materials where are we right now? Eng Fract Mech 2010;77:309–26.
[21] Legay A, Chessa J, Belytschko T. An Eulerian–Lagrangian method for fluid–structure interaction based on level sets. Comput Methods Appl Mech Eng 2006;95(17–18):2070–87.
[22] Legay A, Wang HW, Belytschko T. Strong and weak discontinuities in spectral finite elements. Int J Numer Methods Eng 2005;64:991–1008.
[23] Lerch R. Simulation of piezoelectric devices by two- and three-dimensional finite elements. IEEE Trans Ultrason Ferroelectr Freq Control 1990;37(3):233–47. ISSN 0885-3010.
[24] Melenk JM, Babuška I. The partition of unity finite element method: basic theory and applications. Comput Methods Appl Mech Eng 1996;139(1–4):289–314. ISSN 0045-7825.
[25] Moes N, Dolbow J, Belytschko T. A finite element method for crack growth without remeshing. Int J Numer Methods Eng 1999;46(1):133–50.
[26] Namhoon C, Sunwoo K. Nonlinear modeling and injection rate estimation of common rail injectors for direct injection diesel engines. Trans Soc Automot Eng Jpn 2006;37(1):49–54.
[27] Nguyen-Xuan H, Liu GR, Nguyen-Thoi T, Nguyen Tran C. An edge based smoothed finite element method (ES-FEM) for analysis of twodimensional piezoelectric structures. J Smart Mater Struct 2009;18:065015.
[28] Nguyen-Xuan H, Nguyen-Thoi T, Tran Loc V. Analysis of functionally graded plates using an edge-based smoothed finite element method. Compos Struct 2011;93:3019–39.
[29] Pak YE. Linear electro-elastic fracture mechanics of piezoelectric materials. Int J Fract 1992;54:79100.

[30] Park SB, Sun CT. Fracture criteria for piezoelectric ceramics. J Am Ceram Soc 1995;78:1475–80.
[31] Rabczuk T, Zi G, Bordas S, Nguyen-Xuan H. A simple and robust three dimensional cracking-particle method without enrichment. Comput Methods Appl Mech Eng 2010;199(37-40):2437–55.
[32] Rabinovich D, Givoli D, Vigdergauz S. XFEM-based crack detection scheme using a genetic algorithm. Int J Numer Methods Eng 2007;71:1051–80.
[33] Rabinovich D, Givoli D, Vigdergauz S. Crack identification by arrival time using XFEM and a genetic algorithm. Int J Numer Methods Eng 2009;77:337–59.
[34] Rao BN, Kuna M. Interaction integrals for fracture analysis of functionally graded piezoelectric materials. Int J Solids Struct 2008;4:5237–57.
[35] Réthoré J, Gravouil A, Combescure A. A combined space–time extended finite element method. Int J Numer Methods Eng 2005.
[36] Réthoré J, Gravouil A, Combescure A. An energy-conserving scheme for dynamic crack growth using the extended finite element method. Int J Numer Methods Eng 2005.
[37] Shindo Y, Tanaka K, Narita F. Singular stress and electric fields of a piezoelectric ceramic strip with a finite crack under longitudinal shear. Acta Mech 1997;120:3145.
[38] Sosa HA. On the fracture mechanics of piezoelectric solids. Int J Solids Struct 1992;29:2613–22.
[39] Strouboulis T, Babuška I, Copps K. The design and analysis of the generalized finite element method. Int J Numer Methods Eng 2000;181:43–69.
[40] Strouboulis T, Copps K, Babuška I. The generalized finite element method: an example of its implementation and illustration of its performance. Int J Numer Methods Eng 2000;47(8):1401–17.
[41] Suo Z, Kuo CM, Barnett DM, Willis JR. Fracture mechanics for piezoelectric ceramics. J Mech Phys Solids 1992;40:739–65.
[42] Verhoosel CV, Remmers JJC, Gutierrez MA. A partition of unity-based multiscale approach for modelling fracture in piezoelectric ceramics. Int J Numer Methods Eng. http://dx.doi.org/10.1002/nme.2792.
[43] Wünsche M, Garcia-Sanchez F, Saez A, Zhang Ch. A 2d time-domain collocation-Galerkin BEM for dynamic crack analysis in piezo electric solids. Eng Anal Bound Elem 2010;45:377–87.
[44] Menk A, Bordas S. Numerically determined enrichment functions for the extended finite element method and their application to polycrystalline structures. Int J Numer Meth Eng 2010;83(7):805–28.
[45] Menk A, Bordas S. Crack growth calculations in solder joints based on microstructural phenomena with X-FEM. Comp Mater Sci 2010;50(3):1145–56.
[46] Menk A, Bordas S. Influence of the microstructure on the stress state of solder joints during thermal cycling. In 10th International Conference on Thermal, Mechanical and Multi-Physics simulation and Experiments in Microelectronics and Microsystems, 2009. EuroSimE 2009, pages 1–5, 2009.
[47] Rabczuk T, Bordas S, Zi G. On three-dimensional modelling of crack growth using partition of unity methods. Comput Struct 2010;88(23–24):1391–411.
[48] Natarajan S, Baiz PM, Bordas S, Rabczuk T, Kerfriden P. Natural frequencies of cracked functionally graded material plates by the extended finite element method. Comp Struct 2011;93(11):3082–92.
[49] Bordas S, Natarajan S, Dal Pont S, Rabczuk T, Kerfriden P, Mahapatra DR, et al. On the performance of strain smoothing for enriched finite element approximations (XFEM/GFEM/PUFEM). Int J Numer Meth Eng 2011;86(4-5):637–66.
[50] Rabczuk T, Gracie R, Song JH, Belytschko T. Immersed particle method for fluid structure interaction. Int J Numer Meth Eng 2010;81(1):48–71.
[51] Rabczuk T, Areias PMA, Belytschko T. A meshfree thin shell method for nonlinear dynamic fracture. Int J Numer Meth Eng 2007;72(5):524–48.
[52] Duddu R, Bordas S, Moran B, Chopp D. A combined extended finite element and level set method for biofilm growth. Int Journal Numer Meth Eng 2008;74:848–70.
[53] Simpson RN, Bordas S, Asenov A, Brown AR. Enriched residual free bubbles for semiconductor device simulation. Comput Mech 2012:1–15. http://www.springerlink.com/content/b7vvq5415w675670/.
[54] Bordas S, Nguyen PV, Dunant C, Guidoum A, Nguyen-Dang H. An extended finite element library. Int J Numer Meth Eng 2007;71(6):703–32.
[55] Nguyen VP, Rabczuk T, Bordas S, Duflot M. Meshless methods: review and key computer implementation aspects. Math Comput Simulat 2008;79:763–813. http://dx.doi.org/10.1016/j.matcom.2008.01.003.